Current Control in Field-Excited Flux Switching Machines: No-Load Induced Voltage Impact Based on the Winding Connection

Diogo P. V. Galo [1,*], **Thales A. C. Maia** [2], **Braz de J. Cardoso Filho** [2]

[1]Universidade Federal de Minas Gerais, Graduate Program in Electrical Engineering, Belo Horizonte - Minas Gerais, Brazil.
[2]Universidade Federal de Minas Gerais, Department of Electrical Engineering, Belo Horizonte - Minas Gerais, Brazil.

e-mail: diogogalo23@hotmail.com* ; thales@ufmg.br; braz.cardoso@ieee.org
*Corresponding author

ABSTRACT Micro and mild hybrid electric vehicles can make a significant contribution to reducing emissions and mitigating the environmental impact. Electric machine designs with fewer or no rare-earth permanent magnets will play an important role in the adoption of hybrid solutions. Doubly salient reluctance machines exhibit a simple structure, robust mechanical strength, excellent fault tolerance, and a wide range of speed regulation, which makes them suitable for in-wheel applications. Particular emphasis should be placed on flux-switching machines with wound-field excitation, which offer great operating flexibility, efficient heat dissipation, and power density of up to 4.8 kW/kg. This paper introduces a wound-field flux-switching machine designed for in-wheel applications, featuring individual field current control. The machine has individual access to each of the field coils. The primary objective of this research is to enhance the machine's operational versatility by enabling multiple configurations of the machine, adjusting the way the field-coils are connected. Firstly, a comparison of the armature no-load induced voltage is made for field coils connected in both series and parallel. Additionally, an assessment of the impact of open-circuit failures in one and two adjacent field coils is conducted. Finally, a current control strategy is proposed to effectively manage each individual field coil.

KEYWORDS Would-field flux-switching machine, in-wheel drives, hybrid electric vehicles, independent field current control.

I. INTRODUCTION

The need to minimize the environmental impact of internal combustion engines has stimulated recent changes in the automotive industry, which must now follow a sustainable development path to minimize its negative effects on nature. [1].

As Figure 1 projects, the combined share of sales of internal combustion engine (ICE) light-duty vehicles (LDV) — including gasoline, diesel, flex-fuel, natural gas, and propane powertrains — will decrease from 92% in 2021 to 79% in 2050 because of the growth in sales of battery electric vehicles (BEVs), plug-in hybrid-electric vehicles (PHEVs), and hybrid-electric vehicles (HEVs). Despite the increase in sales of electric and hybrid vehicles, gasoline will remain the dominant light-duty vehicle propulsion fuel by 2050 [2].

Several technologies have been applied to produce more efficient engines in order to comply with the forthcoming regulations [3]. Even with such improvements, especially in developing countries, emission standards will continue to require advancements in current vehicle technology. The most direct and effective solution is to replace traditional combustion engines with modern, highly efficient, and emission-free electric drives.
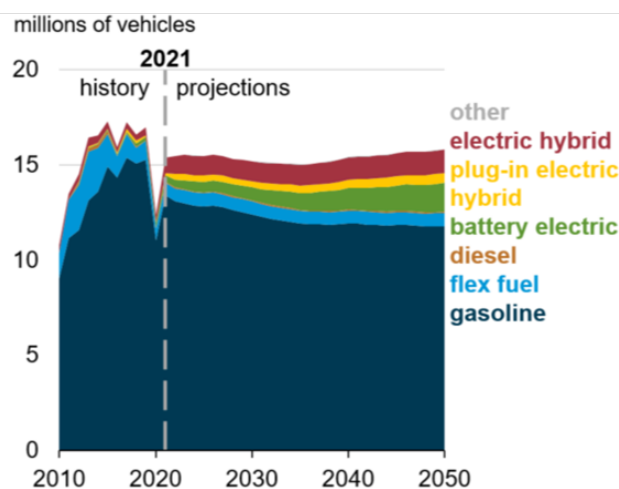
FIGURE 1. Light-duty vehicle sales by technology or fuel [2].

Electrification is inevitable for carbon neutrality in transport. In addition to climate damage, sticking to carbon fuels would isolate a country from the global industry, which would seriously affect its competitiveness and access to

technology. However, most developing countries are not ready to shift abruptly to pure battery electric vehicles, as most of their population would be unable to afford them, and the massive investment in infrastructure is beyond their current capacity [4].

In the meantime, there is plenty of unused or wasted energy in vehicular applications that can be harvested and further used to improve fuel economy, reduce emissions, and supply power to other systems [5].

In light-duty passenger vehicles, energy can be harvested using different techniques, with regenerative braking being one of the most common methods for this purpose [6]. The kinetic energy that would be dissipated by the mechanical brakes can be recovered during deceleration and used to power electric and electronic loads on the vehicle or even assist with propulsion. The energy can be recovered by placing electric generators inside the wheels of a vehicle, commonly called in-wheel electric motors or electric motor-hubs.

The design of an electric motor dedicated for assembly inside the wheels opens up a whole new vista of opportunities for the automobile industry. The new possibilities of such a solution include the elimination of elements of the drive mechanisms used to transfer the torque between the electric motor and the wheel, increasing the efficiency of the entire drive, as well as allowing for more dynamic driving and turning, and new designs of hybrid drives [7].

In traditional electric machines used for in-wheel applications, the excitation sources are usually concentrated on the rotor. These machines, such as the permanent magnet synchronous machine (PMSM), have high power density and efficiency and have been widely used.

However, the permanent magnets placed on the rotor usually require special reinforcement measures to overcome the centrifugal force during high-speed operation, leading to a complex machine structure and high manufacturing cost. Moreover, the poor heat dissipation capacity of the machine leads to an increase in the surface temperature of the rotor, which may cause irreversible demagnetization of the permanent magnets. Consequently, numerous researchers are actively directing their efforts towards exploring alternatives with less or no rare-earth materials for traction drives [8].

Doubly salient reluctance machines are widely studied in the literature due to their great flexibility in both stator and rotor structures. In these types of machines, the flux sources are placed on the stator, leaving the rotor completely passive. This feature is especially interesting in in-wheel applications where heat dissipation can be troublesome due to space constraints, excessive heat from the mechanical brakes, and harsh working conditions such as mud or clay. Among various designs, the variable flux reluctance motor (VFRM) and flux-switching machine (FSM) are known for their ability to enhance torque production with the aid of DC excitation coils [9].

In the VFRM, there exist two sets of windings on the stator, comprising field excitation and armature coils. To further simplify the stator configuration, it is possible to combine the field and armature coils in many different ways. The armature and field coils are usually concentrated and concentric. In this type of machine, employing integrated field and armature current control can significantly enhance torque output capacity and drive efficiency, offering a noteworthy improvement [10].

Liu et al. [11] present a phase angle control strategy for fault-tolerant operation in a 12-slot-14-rotor-pole (12s14r) modular VFRM, where the control sequence is optimized to achieve the maximum output power of the generation system. For faults in an armature winding, it cuts off the faulty module and increases the field current of the normal modules. For faults in the field winding, it disconnects the excitation circuit and optimizes the control angle of the power switches to maximize the output power.

The flux-switching machine usually has overlapping field and armature windings. Bipolar flux is generated by the rotation of the salient pole rotor organized with exciting DC field on the stator, and therefore, in the AC windings, back EMF can be produced. Hence, when AC windings are supplied by bipolar currents, electromagnetic torque is produced [12].

Alternatively, the FSM field can be generated purely by permanent magnets or combined with field coils. PM-type FSMs, which generally have high torque density and high efficiency comparable to those of conventional PM ac machines, have been developed for applications such as power tools, electric vehicles, and aerospace products. However, PM materials carry a risk of demagnetization when the motor operates at high speeds and temperatures [13].

FSM machines have been widely discussed in the literature with particular emphasis on machine optimization design, cost-effectiveness, reducing permanent magnet content, and fault tolerance [14]–[19]. However, only a few studies have investigated the field current control in each of the excitation coils.

In a previous work, a wound-field flux-switching machine (WF-FSM) for in-wheel applications was re-build in order to make it possible independent access to each of the field coils [20]. A independent current control approach was presented, however the impact of each type of connection (parallel, series and individual control) was only simulated but not verified experimentally.

This paper presents an experimental validation of the individual access to each field coil and present the impact in the no-load armature induced voltage depending on the way the connections of the field coils are made. The induced voltage is analysed in terms of the waveform harmonics and total harmonic distortion. Additionally, an assessment of the impact of open-circuit failures in one and two adjacent field coils is conducted. At the event, a current control approach based on the field circuit dynamics is presented.

II. CASE STUDY: WOUND-FIELD FLUX-SWITCHING MACHINE

A. Overview

The main advantage of WF-FSM machines compared to induction machines, synchronous machines, direct current machines, etc., is that all the active parts such as armature coils and field excitation coils are located on the stator, while the rotor consists of only iron material without windings [21].

In [22], the design, optimization, and performance analysis of a 12-slot-10-pole wound-field flux-switching machine are carried out for use in a hybrid electric vehicle. With current densities of up to 21 A/mm^2, the proposed machine was able to achieve a power density of up to 4.8 kW/kg and 210 N.m of torque. Also, given its robust rotor structure, the maximum achievable motor speed reached up to 20,000 rpm. The results showed that the machine is a suitable candidate to compete with interior permanent magnet synchronous motors.

An in-wheel wound-field flux-switching machine presented in [23] is designed to operate as a generator for harvesting energy during deceleration. The machine was designed to be placed on the rear wheels of a light-duty passenger vehicle. The machine has 10 rotor poles and 24 slots, with 12 armature coils and 12 field coils, and was designed to operate at low voltages in micro or mild hybrid vehicles. The machine's stator is presented in Figure 2-a, while its rotor is presented in Figure 2-b.
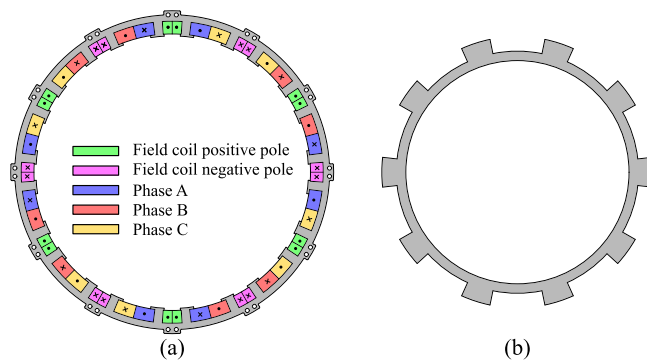
FIGURE 2. Cross-section view of the machine: a) stator b) rotor [23].

Each of the field coil slots is consistently positioned at the center of each corresponding armature coil slot. In a technical sense, direct electrical current is applied to the field coils to establish six south poles interspersed with six north poles. When the system is stationary, the magnetic fields generated circulate around the rotor poles, forming a complete cycle. As the rotor begins to turn, the magnetic field polarity is alternately changed by tracking the rotor pole position. The three-phase armature coils are evenly distributed at regular intervals within the stator body. When the rotor initiates its rotation, the magnetic fluxes generated by the magnetomotive force (MMF) of the field coils start to connect with the armature coils.

Typically, field control in flux switching machines involves adjusting the field current through a series or parallel connection of the coils. However, the series connection can pose challenges, particularly in specific machine configurations. For example, in the machine presented in [23], a series connection would require a voltage as high as 180 V on the field circuit, which would disqualify the vehicle as a low-voltage micro-hybrid. Alternatively, connecting the field coils in parallel has been observed to reduce the induced voltage by 54.8%. The simulated waveforms for the armature induced voltage when the field coils are connected both in series and in parallel are shown in Figure 3.
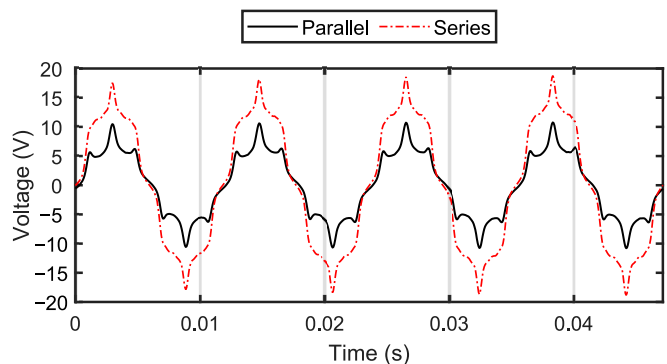
FIGURE 3. Comparison between the induced voltage for parallel and series field coil's connection [23].

Motivated by the observed electromagnetic coupling effect in [23] and the independent current control method presented in [20], this research aims to validate experimentally in the aforementioned papers and characterize the impact of each of field circuit connections in the armature no-load induced voltage.

B. Machine Parameters

To perform the individual current control of each excitation field coil of the flux-switching machine, the prototype presented in [23] was rebuilt to allow access to each coil. All the machine properties were kept the same. The values of inductance for direct and quadrature axis were added. The main machine parameters are shown in Table 1.

C. Field Current Control Drive Topology

The power electronics scheme for driving the WF-FSM in the proposed application is depicted in Figure 4, where SA1 to SA6 are the power switches for the armature, and SF1 to SF24 are the power switches for the field windings.

The stator inverter is composed of 3 H-bridge inverters. Each H-bridge inverter delivers power to one stator winding, so each winding can be controlled independently. Similarly, multiple H-bridges are designed to independently deliver power to each of the 12 field coils in the machine. This configuration enables precise control over both the magnitude and direction of the magnetic field. It becomes feasible to modify the flux generated in the air-gap, thereby

TABLE 1. Machine Parameters [23]

Parameter	Value	
Axial length	51	mm
Airgap radius	134	mm
Airgap lenght	0.5	mm
Stator external radius	148.85	mm
Stator inner radius	136.35	mm
Rotor inner radius	119.15	mm
Number of turns - Armature	15	
Number of turns - Field	840	
Field coil resistance	39	Ω
Field coil L_d	736.3	mH
Field coil L_q	283.8	mH
Rated field current	600	mA

altering the number of poles of the machine. In addition, the proposed scheme will allow the machine to operate in a wide range of operations while adjusting the field current for field weakening characteristics.
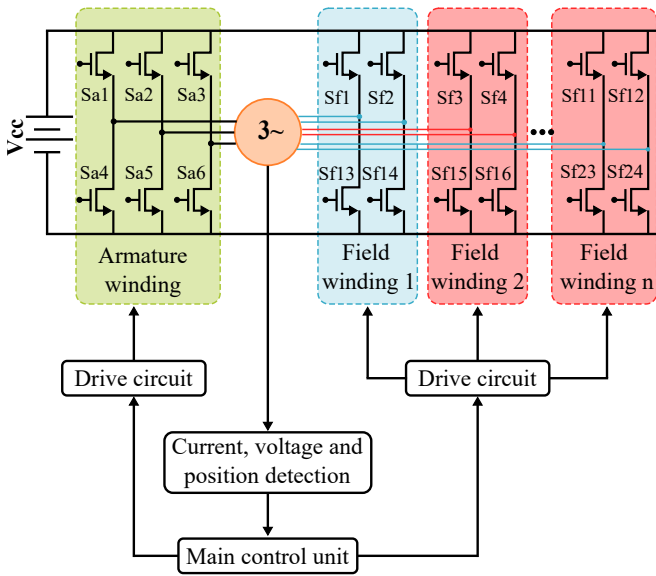
FIGURE 4. Proposed drive diagram for controlling the field coils separately.

The current control board has been specifically designed for the intended application, where each field winding current is rated at 600 mA. To ensure the optimal decoupling effect, precise current alignment among all field coils is necessary. To achieve this, a closed-loop current control system is implemented using the DRV8876 driver. The DRV8876 is a versatile motor driver integrated circuit designed for delivering precise and efficient control for inductive loads across diverse applications. Its key functionalities include bidirectional operation, current sensing capabilities, and built-in protective measures, allowing it to efficiently drive the field coils with currents of up to 1.3 A.

The current control was implemented in [20] using an Espressif Systems ESP32 development board. The DVR8876 has a current-sense output of 1000 μA/A, which is connected to a 2.49 $k\Omega$ resistor, providing a 2.5 V/A output. For a rated current of 1.3 A, the driver will provide adequate voltage to the ADC 3.3 V pin of the development board. The current micro-controller setpoint is provided with the aid of a supervisory software using Wi-Fi and MQTT protocol.

III. FIELD CIRCUIT CONNECTIONS: EXPERIMENTAL VALIDATION

A. Series x Parallel

The test bench described in [20] was enhanced to experimentally validate the no-load induced voltage under various scenarios. The test bench setup is shown in Figure 5. It consists of a voltage source from Itech with a rated voltage of 500 V and 120 A, used to feed the field circuit. The series connection requires voltage levels up to 200 V. The setup also includes a power source from Regatron to supply the inverter for the PMSM machine, with a rated voltage of 65 V and 600 A. The drive system responsible for operating the device under test is a GVM210-100T6 PMSM motor driven by a GVI-E096-0700 inverter.
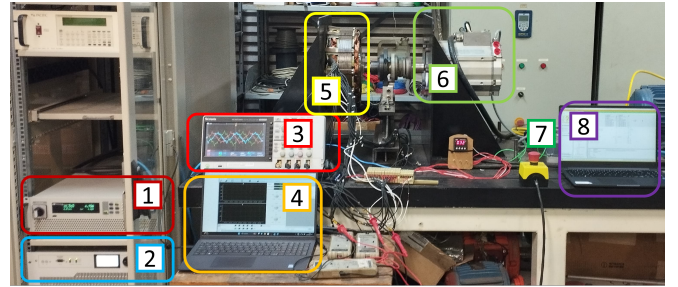
FIGURE 5. Proposed test bench: 1 - 500 V, 120 A power source; 2 - 65 V, 500 A power source; 3 - four channel oscilloscope; 4 - power source software controller; 5 - WF-FSM; 6 - PMSM; 7 - Inverter and CAN-FD adapter; 8 - inverter software controller

The WF-FSM is placed on the test bench as the device under test and is coupled with a PMSM featuring precise torque control, ensuring a comprehensive characterization of the machine across a wide range of operating speeds. An HBM T40B torque transducer with an embedded encoder provides position and speed feedback, facilitating the effective implementation of field-oriented control in future applications.

Firstly, the no-load armature induced voltage with the field circuit connected in series was tested. Measurements were taken for the three-phase voltages. The voltages were recorded for a field current of 400 mA, which required a voltage of 176.8 V. The results were obtained for speeds ranging from 100 rpm to 500 rpm in 100 rpm increments.

In a second test, all the field windings were connected in parallel, resulting in an equivalent resistance of 3.3 Ω. A voltage of 15.6 V was applied to obtain a current of 400 mA in each of the field coils. The results were also

taken for speeds ranging from 100 rpm to 500 rpm in 100 rpm increments. A comparison between the no-load induced voltages for series and parallel field coils connection is depicted in Figure 6 for 500 rpm. Vx-1 are the waveforms for the series connection while Vx-2 are for the parallel connection.
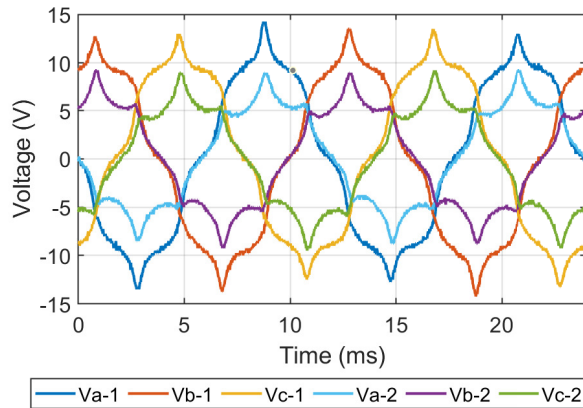
FIGURE 6. Induced Voltage comparison for a field current of 400 mA in each coil and speed of 500 rpm. Vx-1 - Series; Vx-1 - Parallel.

The experimental results obtained for the armature no-load induced voltage reveal important insights into the performance of the FSM under different field coil configurations. Regarding the peak value, the series configuration of the field coil led to an amplitude 50% higher compared to the parallel connection.

Additionally, this configuration exhibited a notable impact from harmonics. The parallel connection introduced more pronounced harmonic distortions in the voltage waveform, which can affect the overall performance and efficiency of the machine. To quantify the harmonic content, the total harmonic distortion value was measured and found to be 10.65% for the parallel connection compared to 15.71% in the series connection.

Figure 7 presents a comparison of the harmonic spectrum for the two types of connection. The fundamental frequency is 83.33 Hz (500 rpm).

A reduction of 38.55% is observed in the fundamental frequency of 83.33 Hz (500 rpm). This reduction rate is consistent across most harmonics, except for the 5th and 13th, which show increases of 132.5% and 14%, respectively.

B. Faults in Field Coils

A test was conducted to evaluate the impact of faults in individual field coils. The first test involved opening Field Coil 1 while keeping the remaining coils operational. Results were recorded for speeds from 100 rpm to 500 rpm in 100 rpm increments. In the second test, both Field Coil 1 and Field Coil 2 (adjacent coils) were opened to assess
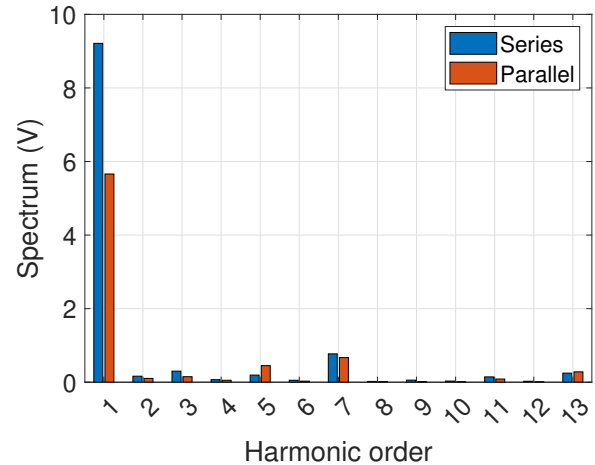
FIGURE 7. Harmonic content comparison for field winding connection in series and parallel.

the combined effect of multiple faults. Measurements were similarly taken across the same speed range.

The comparison of no-load induced voltages for these scenarios reveals how faults in the field coils affect performance. The results, shown in Figure 8, illustrate the variations in induced voltage under different fault conditions and demonstrate the machine's sensitivity to coil failures for a field current of 400 mA and a speed of 500 rpm.
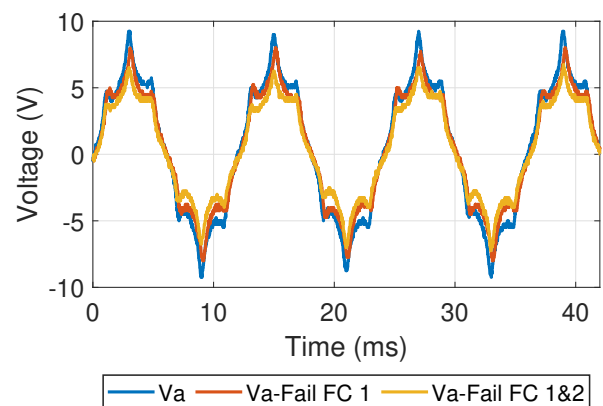
FIGURE 8. Induced Voltage comparison for a field current of 400 mA in each coil and speed of 500 rpm. Va - parallel; Va-Fail FC1 - Field coil 1 with open circuit; Va-Fail FC2 - Field coil 1 and 2 with open circuit.

Regarding the peak value of the induced voltage, the fault condition of Coil 1 resulted in a reduction of 11.1%, while the fault condition of Coils 1 and 2 together led to a reduction of 30.6% compared to the non-fault condition. In terms of THD, the fault condition with Coil 1 had a value of 16.35%, whereas the fault condition with Coils 1 and 2 showed a value of 16.84%.

Figure 9 presents a comparison of the harmonic spectrum for the two fault conditions with open circuit and the parallel connection of the field winding. The fundamental frequency is 83.33 Hz or 500 rpm.
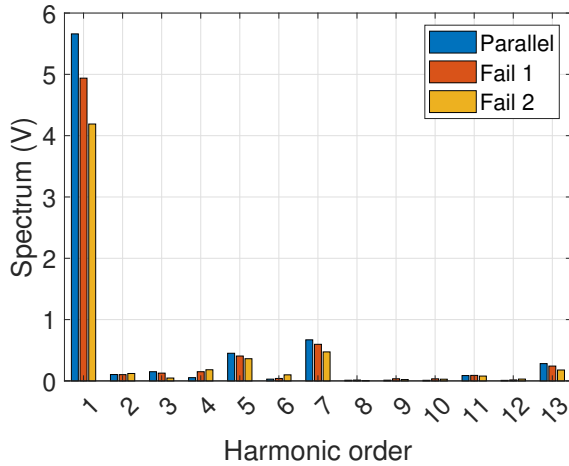
FIGURE 9. Harmonic content comparison for field windings under open-circuit fault.

For the first case, in which a open-circuit fault condition was emulated in the field coil 1, a reduction of 12.76% in the fundamental harmonic was observed. A similar reduction was observed in most even harmonics. Meanwhile, the the 4th, 9th, and 10th, exhibit significant increases of 183.02%, 191.67%, and 240.00%, respectively.

In the second case, in which a open-circuit fault condition was emulated in two adjacent field coils, the fundamental amplitude decreased in 26%. The amplitude rates exhibit reductions in most harmonics, except for the 2nd, 4th, 6th, 9th, 10th, and 12th, which show increases of 16.35%, 243.40%, 241.38%, 83.33%, 180.00%, and 233.33%, respectively.

IV. CURRENT CONTROL ANALYSIS

The current control strategy proposed in [20] was evaluated under no-load conditions. The test setup aimed to maintain a field current of 400 mA in each coil, with rotational speeds varying from 100 to 500 rpm in 100-rpm increments. The idea is to utilize the prototype control board from the previous work, shown in Figure 10.

However, when the PI control strategy from [20] was applied to the WF-FSM using the test bench shown in Figure 5, it was observed that the control method and associated hardware were ineffective in maintaining the field current at the desired setpoint. The actuator saturates when trying to regulate the field current as the rotor's north pole passes through the corresponding field coil. Further investigation is detailed in the next section.

V. PROPOSED CURRENT CONTROL

The proposed field current control strategy accounts for the field coil circuit to enhance performance and stability.
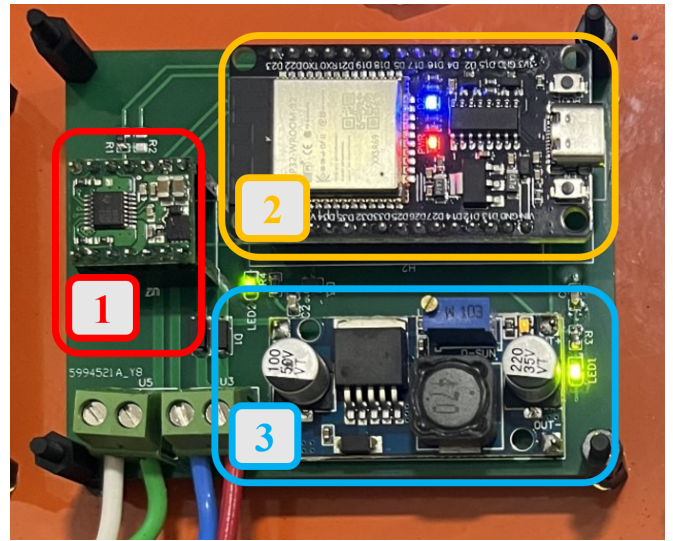
FIGURE 10. PCB built for driving the field current: 1 - DVR8876 drive featuring current sensing capabilities; 2 - micro-controller ESP32; 3 - regulated 3.3 V power supply

This control approach addresses a disturbance termed "e," which includes the back-EMF generated by the machine in each of the field coilds. By incorporating the effects of this disturbance, the control system is designed to maintain precise field current regulation. Also, the effect of the voltage drop in the field coil resistance is compensated using the element $\widehat{R}$, which is the estimated magnetization winding resistance.

The block diagram for the control strategy is presented in Figure 11. It features a proportional gain, R_a, and the unit gain block that represents the inverter. Regarding the electric parameters of the machine, L represents the self- and mutual inductances of the machine, L_0 the mean value between the direct and quadrature values of the magnetization inductance, R the resistance of the magnetization winding and ω_0 the angular speed of the machine.
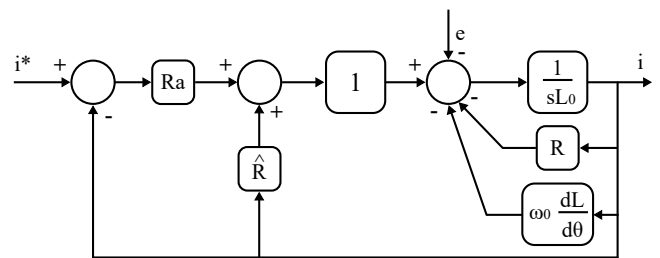
FIGURE 11. Proposed current control.

For calculating the proportional gain, the total disturbance will be accounted for the effect from the mutual and self-inductance and can be represented by e_t in the Eq. 1.

$$e_t = e + \omega_0 \frac{dL}{d\theta} \tag{1}$$

The proportional gain value, R_a, can be obtained from the transfer function from Eq. 2.

$$\left| \frac{e_t}{i} \right| = sL_0 + R_a \qquad (2)$$

Considering $\hat{R} = R$ and L_0 the mean value between L_q and L_d, the proportional gain can be obtained from Eq. 3.

$$R_a = L_0 \cdot 2\pi \cdot f_0 \qquad (3)$$

f_0 represents the chosen cutoff frequency, typically set to one-tenth of the sampling frequency. For the current control board designed in [20], with a sampling frequency of 1 kHz, the calculated proportional gain R_a is 320.5 V/A. Theoretically, this controller should be sufficient to regulate the current at the desired setpoint. However, during experimental validation, several issues were identified. One critical issue is the back-EMF generated in the field coil where the current is to be regulated. As shown in Figure 12, the induced voltage exhibits peaks of up to 20 V.
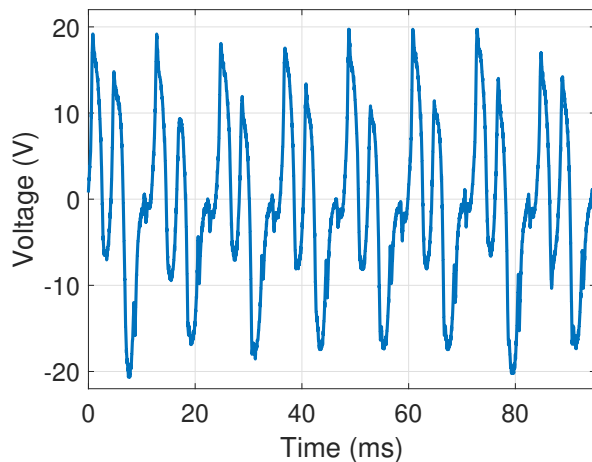
FIGURE 12. Back-EMF measured from one of the field coils.

This measurement was taken with the circuit open, meaning it did not account for the self-inductance of the field coil, which would further increase the amplitude of the back-EMF under dynamic conditions. The hardware depicted in Figure 10 has a maximum output voltage of 37 V, which is insufficient to overcome the back-EMF and achieve the desired setpoint current.

The hardware's sampling frequency is limited to 1 kHz, resulting in a current control loop cutoff frequency of approximately 100 Hz. This limitation significantly reduces the system's ability to respond to rapid variations in the field current, thereby compromising the effectiveness of current regulation.

Finally, after further investigation, it was observed that both the current and back-EMF on the field coil contain significant harmonic content, particularly at frequencies beyond the cutoff frequency of the control loop.

VI. CONCLUSIONS

This study investigates the operational flexibility and fault tolerance of a Wound-Field Flux-Switching Machine designed for in-wheel applications in hybrid electric vehicles. The WF-FSM, featuring independent access to each field coil, offers enhanced versatility by allowing various configurations of coil connections and individualized control. The experimental validation confirms the performance impact of different field coil configurations and faults.

The comparison between series and parallel connections for the field coils revealed that the series connection yields a higher no-load armature induced voltage and exhibits less harmonic distortion compared to the parallel connection. Specifically, the series connection showed a 50% higher peak voltage and a lower THD of 10.65% compared to 15.71% for the parallel connection. These results underscore the importance of configuration in optimizing machine performance.

Testing the effects of open-circuit faults in individual and adjacent field coils demonstrated that such faults significantly reduce the induced voltage and impact harmonic content. The presence of a fault in one coil reduced the induced voltage by 11.1%, while faults in two adjacent coils led to a 30.6% reduction. The machine should be able to be fault tolerant, but performing at a lower level. The dynamic behavior of this condition was not analyzed in this paper.

Finally, the current control proposed in the previous work was tested on the existing hardware, which revealed significant limitations. To address these challenges in future studies, two key aspects must be improved: first, the development of hardware with an adequate sampling rate and sufficient supply voltage; second, the implementation of advanced control strategies, such as resonant PR controllers, adaptive control, or similar approaches, to effectively manage harmonic components and improve current regulation.

AUTHOR'S CONTRIBUTIONS
D. P. V. GALO: Conceptualization, Data Curation, Formal Analysis, Investigation, Methodology, Software, Validation, Visualization, Writing – Original Draft, Writing – Review & Editing. **T. A. C. MAIA**: Formal Analysis, Project Administration, Supervision, Visualization. **B. J. CARDOSO FILHO**: Formal Analysis, Funding Acquisition, Project Administration, Resources, Supervision, Visualization.

PLAGIARISM POLICY
This article was submitted to the similarity system provided by Crossref and powered by iThenticate – Similarity Check.

REFERENCES

[1] A. C. T. Malaquias, N. A. D. Netto, F. A. R. Filho, R. B. R. da Costa, M. Langeani, J. G. C. Baêta, "The misleading total replacement of internal combustion engines by electric motors and a study of the Brazilian ethanol importance for the sustainable future of mobility: a review", *Journal of the Brazilian Society of Mechanical Sciences and Engineering*, vol. 41, pp. 1–23, 2019, doi:https://doi.org/10.1007/s40430-019-2076-1.

[2] S. Nalley, A. LaRose, "Annual energy outlook 2022 (AEO2022)", *Energy Information Agency*, vol. 23, 2022.

[3] L. Lešnik, B. Kegl, E. Torres-Jiménez, F. Cruz-Peragón, "Why we should invest further in the development of internal combustion engines for road applications", *Oil & Gas Science and Technology–Revue d'IFP Energies nouvelles*, vol. 75, p. 56, 2020, doi:https://doi.org/10.2516/ogst/2020051.

[4] C. L. K. Yamamura, H. Takiya, C. A. S. Machado, J. C. C. Santana, J. A. Quintanilha, F. T. Berssaneti, "Electric cars in Brazil: An analysis of core green technologies and the transition process", *Sustainability*, vol. 14, no. 10, p. 6064, 2022, doi:https://doi.org/10.3390/su14106064.

[5] H. Pan, L. Qi, Z. Zhang, J. Yan, "Kinetic energy harvesting technologies for applications in land transportation: A comprehensive review", *Applied Energy*, vol. 286, p. 116518, 2021, doi:https://doi.org/10.1016/j.apenergy.2021.116518.

[6] Y. Zhu, H. Wu, J. Zhang, "Regenerative braking control strategy for electric vehicles based on optimization of switched reluctance generator drive system", *IEEE Access*, vol. 8, pp. 76671–76682, 2020, doi:https://doi.org/10.1109/ACCESS.2020.2990349.

[7] P. Dukalski, R. Krok, "Selected Aspects of Decreasing Weight of Motor Dedicated to Wheel Hub Assembly by Increasing Number of Magnetic Poles", *Energies*, vol. 14, no. 4, p. 917, 2021, doi:https://doi.org/10.3390/en14040917.

[8] Y. Wang, N. Bianchi, R. Qu, "Comparative study of non-rare-earth and rare-earth PM motors for EV applications", *Energies*, vol. 15, no. 8, p. 2711, 2022, doi:https://doi.org/10.3390/en15082711.

[9] Y. Zhao, C. Lu, D. Li, X. Zhao, F. Yang, "Overview of the optimal design of the electrically excited doubly salient variable reluctance machine", *Energies*, vol. 15, no. 1, p. 228, 2021, doi:https://doi.org/10.3390/en15010228.

[10] H. Cheng, J. Zhou, Q. Hu, J. Sun, D. Yu, "General Analysis and Vector Control for Doubly Salient Reluctance Machines", *IEEE Transactions on Power Electronics*, 2023, doi:https://doi.org/10.1109/TPEL.2023.3294604.

[11] Z. Liu, K. Wang, B. Zhou, "Fault-tolerant operation of DC-field excited modular variable flux reluctance machine under open-circuit faults", *IEEE Transactions on Industrial Electronics*, vol. 69, no. 11, pp. 10834–10845, 2021, doi:https://doi.org/10.1109/TIE.2021.3118383.

[12] M. Yousuf, F. Khan, B. Ullah, "Electromagnetic performance of five phase non-overlapping stator wound field flux switching machine", *Journal of Electrical Engineering & Technology*, pp. 1–10, 2022, doi:https://doi.org/10.1007/s42835-021-00915-1.

[13] S.-M. Yang, J.-H. Zhang, J.-Y. Jiang, "Modeling torque characteristics and maximum torque control of a three-phase, dc-excited flux-switching machine", *IEEE Transactions on Magnetics*, vol. 52, no. 7, pp. 1–4, 2016, doi:https://doi.org/10.1109/TMAG.2016.2526620.

[14] B. Wu, D. Xu, J. Ji, W. Zhao, Q. Jiang, "Field-oriented control and direct torque control for a five-phase fault-tolerant flux-switching permanent-magnet motor", *Chinese Journal of Electrical Engineering*, vol. 4, no. 4, pp. 48–56, 2018, doi:https://doi.org/10.23919/CJEE.2018.8606789.

[15] W. Jiang, W. Huang, X. Lin, Y. Zhao, X. Wu, Y. Zhao, D. Dong, X. Jiang, "A novel stator wound field flux switching machine with the combination of overlapping armature winding and asymmetric stator poles", *IEEE Transactions on Industrial Electronics*, vol. 69, no. 3, pp. 2737–2748, 2021, doi:https://doi.org/10.1109/TIE.2021.3063955.

[16] S. Akbar, F. Khan, W. Ullah, B. Ullah, M. Yousuf, S. Hussain, "Comparative Study of Outer Rotor Field Excited Flux Switching Machine with Feasible Rotor Poles For EV and HEV Application", *in 2022 International Conference on Technology and Policy in Energy and Electric Power (ICT-PEP)*, pp. 174–179, IEEE, 2022, doi:https://doi.org/10.1109/ICT-PEP57242.2022.9988789.

[17] B. Ullah, F. Khan, A. H. Milyani, "Analysis of a discrete stator hybrid excited flux switching linear machine", *IEEE Access*, vol. 10, pp. 8140–8150, 2022, doi:https://doi.org/10.1109/ACCESS.2022.3143794.

[18] Z. Xiang, Z. Lu, X. Zhu, M. Jiang, D. Fan, L. Quan, "Research on magnetic coupling characteristic of a double rotor flux-switching PM machine from the perspective of air-gap harmonic groups", *IEEE Transactions on Industrial Electronics*, vol. 69, no. 12, pp. 12551–12563, 2022, doi:https://doi.org/10.1109/TIE.2021.3139182.

[19] J. Chu, H. Cheng, J. Sun, C. Peng, Y. Hu, "Multi-objective optimization design of hybrid excitation double stator permanent magnet synchronous machine", *IEEE Transactions on Energy Conversion*, vol. 38, no. 4, pp. 2364–2375, 2023, doi:https://doi.org/10.1109/TEC.2023.3279934.

[20] D. P. V. Galo, T. A. C. Maia, B. de Jesus Cardoso Filho, "Independent Field Excitation Control of an In-Wheel Wound-Field Flux-Switching Machine for Micro-Hybrid Applications", *in 2023 IEEE 8th Southern Power Electronics Conference (SPEC)*, pp. 1–6, IEEE, 2023, doi:https://doi.org/10.1109/SPEC56436.2023.10408436.

[21] F. Khan, E. Sulaiman, M. Z. Ahmad, "Review of switched flux wound-field machines technology", *IETE Technical Review*, vol. 34, no. 4, pp. 343–352, 2017, doi:https://doi.org/10.1080/02564602.2016.1190304.

[22] E. B. Sulaiman, F. Khan, T. Kosaka, "Field-excited flux switching motor design, optimization and analysis for future hybrid electric vehicle using finite element analysis", *Progress In Electromagnetics Research B*, vol. 71, pp. 153–166, 2016, doi:http://dx.doi.org/10.2528/PIERB16092502.

[23] G. A. Mendonça, D. P. Galo, L. C. M. Sales, B. J. Cardoso Filho, T. A. Maia, "Design and experimental evaluation of an in-wheel flux-switching machine for light vehicle application", *Machines*, vol. 10, no. 8, p. 671, 2022, doi:https://doi.org/10.3390/machines10080671.

BIOGRAPHIES

Diogo Pereira Vilela Galo born in Brazil in 1989 and is an electrical engineer (2015), master (2018) with Universidade Federal de São João del Rei and is a Ph.D. candidate at Universidade Federal de Minas Gerais. His areas of interest are electrical machines and drives, power electronics and vehicular electrification.

Thales Alexandre Carvalho Maia was born in Brazil in 1984. He received the Ph.D. degree in mechanical engineering from the Universidade Federal de Minas Gerais, Belo Horizonte, Brazil, in 2016.,Since 2009, he has been an Electrical Engineer. His main working fields include electrical machine design and power electronics. He is an Assistant Professor with the Department of Electric Engineering, Universidade Federal de Minas Gerais.

Braz de Jesus Cardoso Filho Braz de Jesus Cardoso Filho received the electrical engineer and master of electrical engineering degrees from the Universidade Federal de Minas Gerais, Belo Horizonte, Brazil, in 1988 and 1991, respectively, and the Ph.D. degree in electrical engineering from the University of Wisconsin.Madison, Madison, WI, USA, in 1998.,Since 1989, he has been in a faculty position with the Department of Electrical Engineering, School of Engineering, Universidade Federal de Minas Gerais, where he is currently a Professor of electrical engineering. He is the Founder and Head of the TESLA Power Engineering Laboratory (formerly the Industry Application Laboratory), Universidade Federal de Minas Gerais. He has authored or coauthored more than 200 technical papers on the topics of power electronics and electrical drives, and holds nine patents and patent applications. His research interests include utility applications of power electronics, renewable energy sources, semiconductor power devices, electrical machines and drives, and vehicle electrification.

8

Eletrônica de Potência, Rio de Janeiro, v. 30, e202515, 2025.